Applied Catalysis B: Environmental 95 (2010) 153–159

Contents lists available at ScienceDirect

Applied Catalysis B: Environmental

journal homepage: www.elsevier.com/locate/apcatb

Novel synthesis and high visible light photocatalytic activity of SnS_2 nanoflakes from $SnCl_2{\cdot}2H_2O$ and S powders

Yong Cai Zhang [a,*], Zhen Ni Du [a], Shi Yin Li [b], Ming Zhang [a,*]

[a] Key Laboratory of Environmental Material and Environmental Engineering of Jiangsu Province, College of Chemistry and Chemical Engineering, Yangzhou University, Yangzhou 225002, China
[b] School of Chemistry and Environmental Science, Nanjing Normal University, Nanjing 210046, China

ARTICLE INFO

Article history:
Received 29 August 2009
Received in revised form 9 December 2009
Accepted 17 December 2009
Available online 28 December 2009

Keywords:
Semiconductors
Tin disulfide
Nanomaterials
Photocatalysis

ABSTRACT

A novel method based on heating the mixture of $SnCl_2{\cdot}2H_2O$ and excess S powders in air at 200–240 °C for 0–10 h (t = 0 h, that is, the heating of the reactants was stopped immediately once temperature reached the designed degree), coupled with a subsequent washing treatment, was proposed for the synthesis of SnS_2 nanoflakes. X-ray diffraction, transmission electron microscopy, selected area electron diffraction and Raman spectra revealed the formation of bulk-pure hexagonal phase SnS_2 nanoflakes. UV–vis diffuse reflectance spectra disclosed that the as-synthesized SnS_2 nanoflakes had optical bandgaps in the range of about 2.21–2.25 eV. Besides, the photocatalytic performances of the as-synthesized SnS_2 nanoflakes were evaluated by degrading methyl orange (MO) in deionized water under both the visible light ($\lambda > 420$ nm) and real sunlight irradiation. The results demonstrated that all the SnS_2 products had high visible light photocatalytic activity, and the most efficient photocatalyst among them was the one synthesized at 200 °C for 0 h, which was able to achieve a MO degradation ratio of nearly 100% after 60 min illumination in the first cycle and 86% in the fifth cycle (each cycle lasted for 120 min). Moreover, the best sample also possessed much higher photocatalytic activity than the commercial Degussa P25 TiO_2 photocatalyst under the real sunlight irradiation, and can be easily recovered from the suspension by filtration after the photocatalysis.

1. Introduction

Currently, there has been an extensive interest in the application of semiconductors as photocatalysts to degrade organic pollutants, which are harmful to the environment, hazardous to human health, and difficult to degrade by natural means [1–5]. TiO_2 is undoubtedly the most popular and widely used photocatalyst, in view of its low cost, high photocatalytic activity, chemical and photochemical stability, and biocompatibility. However, it is only active under ultraviolet light irradiation due to its wide bandgap (3.2 eV), not responding to visible light ($\lambda > 400$ nm), which is the main component in solar light and indoor irradiations [1]. For this reason, TiO_2 is limited for large-scale industrial applications and indoor use. Hence, the quest for efficient visible light-sensitive photocatalysts becomes very attractive in this field nowadays [1–5].

SnS_2 has a CdI_2-related crystal structure, consisting of two layers of hexagonal closed packed sulfur anions with sandwiched tin cations which are octahedrally coordinated by six nearest neighbor sulfur atoms. Each S is nested at the top of a triangle of Sn atom. Adjacent S–Sn–S layers are bound by weak van der Waals interactions [6]. It is an n-type semiconductor with a bandgap of 2.18–2.44 eV [7–9], and has good stability in acid and neutral aqueous solutions as well as certain oxidative and thermal stability in air, which makes it a promising visible light-sensitive photocatalyst [5]. In addition, the absence of surface states associated with dangling bonds which could act as recombination centers for photoinjected electrons, makes SnS_2 as an ideal model system for dye sensitization studies and also contributes to the high quantum yields [10]. Besides, SnS_2 also exhibits intriguing electrical, optical and gas sensing properties, and can be used as a candidate material in solar cells and opto-electronic devices [7,8], anode for lithium-ion batteries [11–13], pigment [14], and gas sensor [15], etc. It has been reported that the practical performances of SnS_2 are relative to its crystallinity, morphology, size, crystal defect and surface property, etc., which ultimately depend on the preparation methods and preparation conditions [6–21]. Consequently, so far, great effort has been devoted to designing novel methods for the synthesis of SnS_2 nanomaterials with different characteristics [8–13,15–21], aiming at exploiting their potentials.

* Corresponding author. Tel.: +86 0514 87962581; fax: +86 0514 87975244.
E-mail address: zhangyc@yzu.edu.cn (Y.C. Zhang).

0926-3373/$ – see front matter © 2009 Elsevier B.V. All rights reserved.
doi:10.1016/j.apcatb.2009.12.022

Recently, we have reported the in air synthesis of hexagonal phase SnS_2 microplate particles via the liquid-solid phase reaction of Sn, S and NH_4Cl powders at 250 °C [17], or the molten reaction between $SnCl_2{\cdot}2H_2O$ and thiourea at 250–280 °C [18], without the assistance of template and vacuum environment/inert gas protection. However, in both cases, an impurity phase (ammonium tin chloride: $(NH_4)_2SnCl_6$) would be yielded in the resultant products, implying that the Sn sources (Sn or $SnCl_2{\cdot}2H_2O$) have been partly transformed into $(NH_4)_2SnCl_6$, not completely into SnS_2. Interestingly, we find later day that if $SnCl_2{\cdot}2H_2O$ and excess S powders are used as the reactants, when subjected to heating in air at 200–240 °C for 0–10 h, except the target SnS_2, no other impure phases containing Sn will be produced. Namely, $SnCl_2{\cdot}2H_2O$ can be thoroughly transformed into SnS_2 in such a system, which should be an improvement to the previous methods [17,18]. Moreover, S powder is cheaper (at present, the commercial prices of S and thiourea powders are about 1.3 and 5.6 Chinese Yuan per mole, respectively) and less pollutive than thiourea, and $SnCl_2{\cdot}2H_2O$ is less pollutive than Sn and NH_4Cl, which should be another advantage over the previous methods [17,18]. Herein, we report a novel synthesis of bulk-pure hexagonal phase SnS_2 nanoflakes simply via heating the mixture of $SnCl_2{\cdot}2H_2O$ and excess S powders in air at 200–240 °C for 0–10 h, coupled with a subsequent washing treatment. The structure and optical property of the obtained products are characterized by means of X-ray diffraction (XRD), transmission electron microscopy (TEM), selected area electron diffraction (SAED), Raman and UV–vis diffuse reflectance spectra. Furthermore, their photocatalytic properties are investigated based on the degradation of methyl orange (MO, a common and very stable azo-dye) in deionized water under both the visible light ($\lambda > 420$ nm) and real sunlight irradiation.

2. Experimental

2.1. Synthesis of SnS_2 nanoflakes

All the chemicals used were analytically pure and purchased directly from Sinopharm Chemical Reagent Co., Ltd. In a typical procedure, the powders of 5 mmol tin(II) chloride dihydrate ($SnCl_2{\cdot}2H_2O$) and 20 mmol sublimed sulfur (S) were first mixed and ground in a carnelian mortar for about 15 min, then transferred to a corundum crucible with a cover. The crucibles containing the reactants were heated in an electrothermal oven from room temperature to 200 or 240 °C at an average temperature increase rate of about 4.7 °C/min, kept at 200 or 240 °C for 0–10 h, then the heating was stopped, and the crucibles were allowed to cool to room temperature naturally. The resultant powders were washed with carbon disulfide, deionized water and ethanol to remove the impurities (e.g., the residual S), dried in air at 80 °C, and finally yellow SnS_2 products were obtained.

For the convenience of description, the products synthesized at 200 °C for 0, 5 and 10 h were later called as "200-0 SnS_2", "200-5 SnS_2" and "200-10 SnS_2", respectively, while that synthesized at 240 °C for 0 h was later called as "240-0 SnS_2".

2.2. Characterization

XRD patterns of the obtained products were recorded on a German Bruker AXS D8 ADVANCE X-ray diffractometer at room temperature. TEM and SAED images were taken on a Holland Philips Tecnai–12 transmission electron microscopy. Raman spectra were recorded using a Britain Renishaw Invia Raman spectrometer with a solid-state laser (excitation at 532 nm, 10 mW). UV–vis diffuse reflectance spectra were obtained on a Japan Shimadzu UV-3101PC UV–vis-near infrared spectrophotometer using $BaSO_4$ as reference.

2.3. Photocatalytic tests

Photocatalytic properties of the as-synthesized SnS_2 nanoflakes were studied by following their catalytic degradation of MO in deionized water (10.0 mg/l) under both the visible light ($\lambda > 420$ nm) and real sunlight irradiation. For comparison, the commercial Degussa P25 TiO_2 photocatalyst was also tested under the same conditions. All the photocatalytic experiments under the visible light ($\lambda > 420$ nm) were conducted in triplicates and the results were showed at the mean values.

The visible light photocatalytic experiments were carried out in a specially designed photochemical reactor (see Electronic Supplementary Materials), which includes mainly four parts: an illumination system including an 1000 W Xe lamp, cut-off filter ($\lambda > 420$ nm) and cooling attachment such as air pump and electric fan, reactor (two-layer Pyrex glass bottles of 400 ml capacity, and the space between two layers is filled by a circulating water to cool the reactor), magnetic stirrer and temperature controller. In each experiment, the distance between Xe lamp and Pyrex glass bottles was set to be 10 cm, and the temperature was 20 °C. Before illumination, 300 ml of MO aqueous solutions containing different amounts of SnS_2 nanoflakes were magnetically stirred in the dark for 2 h to permit the adsorption/desorption equilibrium between the photocatalyst and MO. During illumination, about 5.0 ml of suspension was taken from the reaction cell at an interval of time and centrifugated to separate the photocatalyst. The supernatant solution was analyzed by a Japan Shimadzu UV-2550 UV–vis spectrophotometer at the maximum absorption wavelength of MO (462.0 nm). After each photometric measurement, the supernatant solution and photocatalyst were returned to the reaction cell. The measured absorbance intensity of MO aqueous solution at different illumination times was transformed to the degradation ratio, which can be defined as the following expression:

$$\text{Degradation ratio} = \frac{A_o - A_t}{A_o} \times 100\%$$

where A_o and A_t are the absorbance intensities of MO aqueous solution before illumination ($t = 0$ min) and after illumination for t min, respectively.

Photocatalytic tests under the real sunlight irradiation were performed from 10:40 a.m. to 1:40 p.m. on sunny days between 21 November and 24 November, 2009, at latitude 32.39° North and longitude 119.42° East (Yangzhou city, Jiangsu province, China). The temperature throughout these experiments was 13 ± 2 °C. The reaction cells were 1000 ml beakers with a diameter of about 11 cm, which were equipped with a magnetic stirrer. The sunlight photocatalytic procedure was the same as that under the visible light.

3. Results and discussion

3.1. Characterization of the as-synthesized SnS_2 nanoflakes

Fig. 1(a)–(d) show the XRD patterns of the products directly derived from heating the mixture of $SnCl_2{\cdot}2H_2O$ and excess S powders in air at 200–240 °C for 0–10 h. It can be seen that all the products obtained without a subsequent washing treatment comprise a mixture of hexagonal phase SnS_2, orthorhombic phase S_8 (JCPDS card no. 78-1889) and monoclinic phase S (JCPDS card no. 53-1109). In contrast, all the washed products in Fig. 2(a)–(d) display only the XRD peaks corresponding to hexagonal phase SnS_2 (JCPDS card no. 89-2358), meaning that phase-pure SnS_2 powders have been successfully gained after a subsequent washing treatment with carbon disulfide and ethanol. Besides, the impure phases such as $(NH_4)_2SnCl_6$, $SnCl_2$ and Sn, are not detected by the XRD analysis in Fig. 1(a)–(d), indicating a

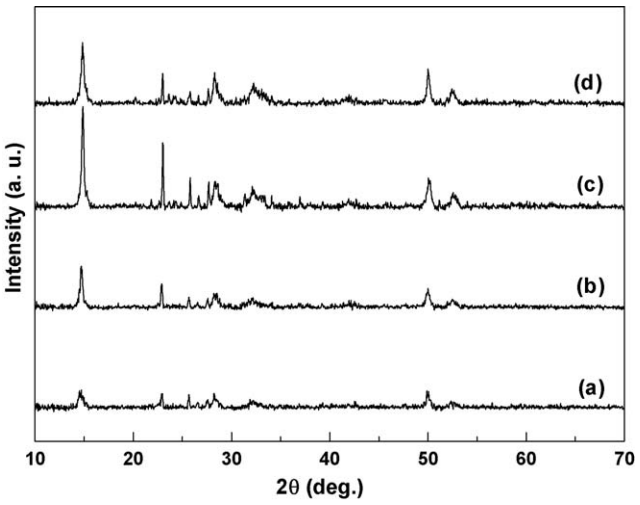

Fig. 1. XRD patterns of the products directly derived from heating the mixture of $SnCl_2{\cdot}2H_2O$ and excess S powders in air at 200 °C for (a) 0, (b) 5 and (c) 10 h, or (d) at 240 °C for 0 h.

complete transformation of $SnCl_2{\cdot}2H_2O$ into SnS_2. It is thought that the fast formation of phase-pure SnS_2 in the current system may at least benefit from the following three factors: first, for the Sn source ($SnCl_2{\cdot}2H_2O$) we use, it melts (that is, $SnCl_2$ dissolves in its own crystal water) at temperature above 38 °C (although $SnCl_2{\cdot}2H_2O$ gradually loses its crystal water at temperature above 100 °C, it can not lose all its crystal water up to 200 °C) [14], and then it (or at least a part of it) reacts with S just as in an aqueous solution; second, in the process of reaction at temperature above 119 °C (the melting point and boiling point of S are around 119 and 445 °C, respectively [14]), the S powder (whose amount is in excess) also becomes molten and participates in the reaction just like a liquid, which certainly increases the interface and contact surface areas between the reactants, and so accelerates the reaction rate; third, the liquid phase reaction between aqueous $SnCl_2$ and excess molten S may also prevent the oxidation of the newly formed SnS_2 by O_2 in air.

Fig. 3(a)–(d) shows the TEM images of the as-synthesized SnS_2 powders, which exhibit overall an anisotropic lamellar morphology. The origin for the formation of flake-like morphology may be strongly related to the intrinsic anisotropic nature of hexagonal phase SnS_2, which adopts a CdI_2-related crystal structure [11,17–19]. The effective flake thicknesses of 200-0 SnS_2, 200-5 SnS_2, 200-10 SnS_2 and 240-0 SnS_2 were calculated to be about 28, 31, 34 and 20 nm, respectively, using the Scherrer equation from the broadening of the (0 0 1) peak in their XRD patterns (Fig. 2(a)–(d)) [11,12]. Besides, the SAED pattern (inserted in Fig. 3(e)) taken from one selected flake (Fig. 3(e)) of 200-0 SnS_2 further indicates the formation of hexagonal phase SnS_2 in single crystal nature.

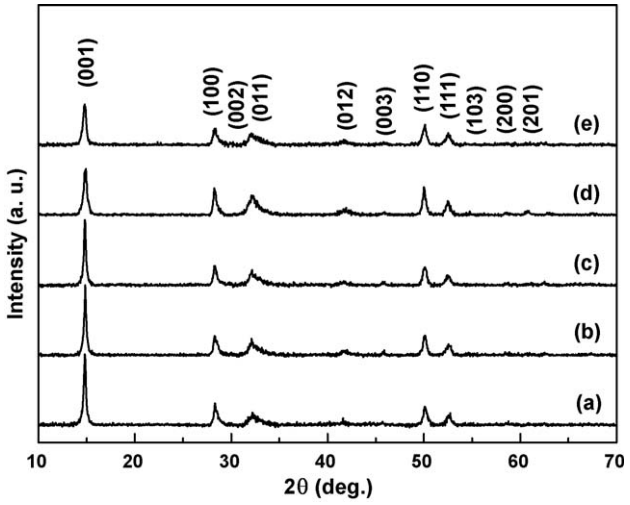

Fig. 2. XRD patterns of the products obtained via heating the mixture of $SnCl_2{\cdot}2H_2O$ and excess S powders in air at 200 °C for (a) 0, (b) 5 and (c) 10 h, or (d) at 240 °C for 0 h, coupled with a subsequent washing treatment; and (e) the product recovered after the fifth cycle photocatalysis.

Fig. 4(a)–(d) shows the Raman spectra of the as-synthesized SnS_2 nanoflakes. All of them exhibit a strong Raman peak at around 310–313 cm^{-1}, which corresponds to the A1 g mode of hexagonal phase SnS_2 [6,8,17–21]. Moreover, no Raman peaks attributable to crystalline SnO_2 are visible in Fig. 4(a)–(d), suggesting a negligible oxidation of the as-synthesized SnS_2 nanoflakes [22]. However, the first-order E_g mode peaked at around 210 cm^{-1} is not observed in the Raman spectra of our products. This phenomenon had also been reported in the literatures [8,17–21], and was attributed to the nanosize effect.

Fig. 5(a) shows the UV–vis diffuse reflectance spectra of the as-synthesized SnS_2 nanoflakes. It can be seen that all the products display optical absorption capabilities nearly in the entire visible light spectrum, which is commonly defined in the range of 400–700 nm. The broad spectrum response suggests that the as-synthesized SnS_2 nanoflakes should be excellent visible light-responsive photocatalysts for degrading organic pollutants (in fact, we have tried the experiment with a cut-off filter of 700 nm in the homemade photochemical reactor, and found that the photocatalytic reactions still progress at a faster speed than those in the dark and blank experiments. So, the incident light with wavelength longer than 700 nm would also be available for the present photocatalytic reactions) [23]. The optical bandgaps are determined based on the theory of optical absorption for direct bandgap semiconductors [7,8]:

$$\alpha h\nu = B(h\nu - E_g)^{1/2}$$

where α is the absorption coefficient, $h\nu$ is the discrete photon energy, B is a constant relative to the material, and E_g is the absorption bandgap. The value of the absorption coefficient can be calculated by the following equation:

$$\alpha = -\frac{1}{t}\ln\frac{I_t}{I_0} = \frac{1}{t}\frac{-\log(I_t/I_0)}{\log e} = \frac{1}{t}\frac{A}{\log e}$$

in which t is the thickness (cm) of the SnS_2 wafers, I_t and I_0 are the intensities of transmitted light and incident light, respectively, and A is the absorbance, which can be obtained from the absorption spectra. The curves of $(\alpha h\nu)^2$ vs $(h\nu)$ for the as-synthesized SnS_2 nanoflakes are plotted in Fig. 5(b). By extrapolating the straight line portion of the plots of $(\alpha h\nu)^2$ vs $(h\nu)$ to $\alpha = 0$, the E_g values of the as-synthesized SnS_2 nanoflakes are estimated to be 2.21–2.25 eV, which fall within the bandgap range reported for SnS_2 single crystals and thin films [7–9].

3.2. Photocatalytic properties of the as-synthesized SnS_2 nanoflakes

Fig. 6 shows the degradation evolution of MO in the presence of 0.3 g of different photocatalysts under the visible light ($\lambda > 420$ nm) irradiation. As can be seen, the synthesis conditions of SnS_2 nanoflakes affect their photocatalytic activities in degrading MO under the visible light irradiation. Among the four SnS_2 products synthesized at 200–240 °C for 0–10 h, 200-0 SnS_2 has the highest photocatalytic activity, which can achieve a MO degradation ratio of 100% within 60 min. The difference in the photocatalytic activities of the four SnS_2 products may be resulted from the combined action of several factors, such as bandgap, size,

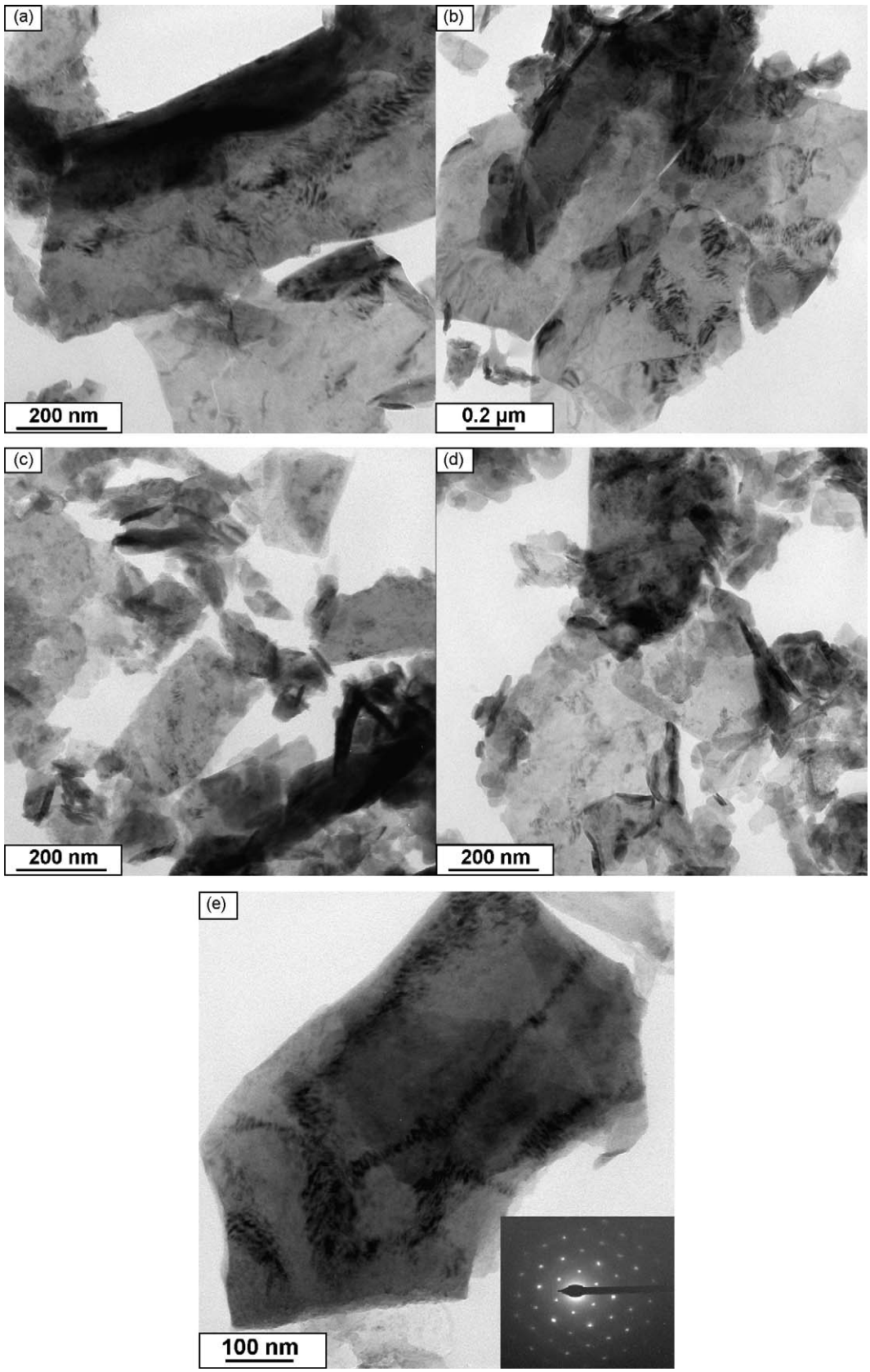

Fig. 3. TEM images of (a) 200-0 SnS_2, (b) 200-5 SnS_2, (c) 200-10 SnS_2, (d) 240-0 SnS_2, and (e) one selected flake (with the corresponding SAED pattern inserted) from 200-0 SnS_2.

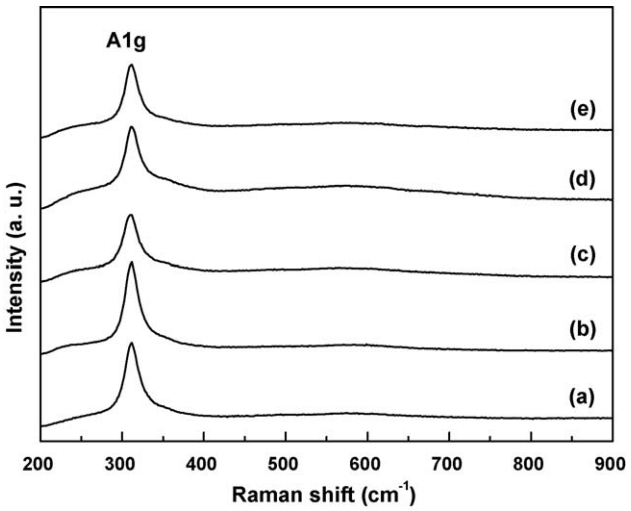

Fig. 4. Raman spectra of the SnS_2 products. *Note*: the products in (a)–(e) correspond to those in Fig. 2(a)–(e).

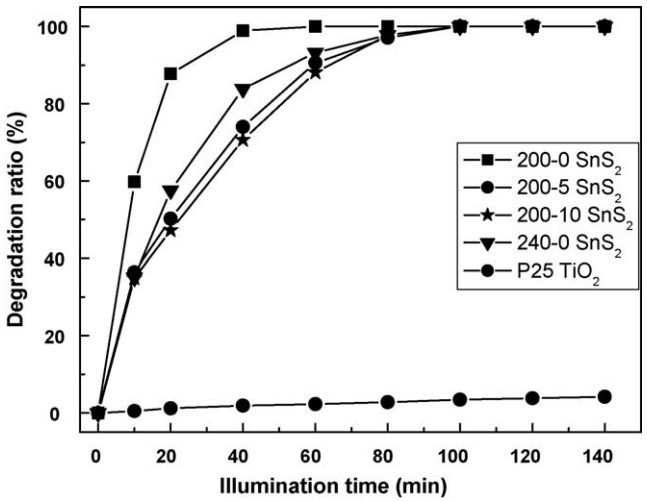

Fig. 6. Degradation evolution of MO over 0.3 g of different photocatalysts under the visible light ($\lambda > 420$ nm) irradiation.

dispersibility, suspensibility, surface area, crystallinity, crystal defects, and photochemical stability, etc. Nevertheless, even the worst product, 200-10 SnS_2 still shows a high efficiency toward the catalytic degradation of aqueous MO under the visible light irradiation. For example, the degradation ratio of MO over 0.3 g of 200-10 SnS_2 approaches 100% when irradiated by the visible light for 100 min. On the contrary, when P25 TiO_2 substitutes for SnS_2 as the photocatalyst, the degradation of MO takes place at a much slower rate under the visible light irradiation. For instance, the degradation ratio of MO is only 3.4% over 0.3 g of P25 TiO_2 when irradiated by the visible light for 100 min.

Fig. 7 shows the degradation evolution of MO in the presence of different amounts of 200-0 SnS_2 under the visible light ($\lambda > 420$ nm) irradiation. It is evident that the degradation ratios of MO are generally improved when the amounts of 200-0 SnS_2 used are increased for a certain illumination time, or when the illumination times are prolonged for a certain amount of 200-0 SnS_2 until the complete degradation of MO. The enhancement in degrading rates of MO with increased concentrations of 200-0 SnS_2 is characteristic of heterogeneous catalysis, and can be rationalized in terms of the availability of active cites on the photocatalyst surface as well as the light penetration of photoactivating light into the suspension [24–28]. But on the whole, 200-0 SnS_2 possesses high photocatalytic capability under the visible light irradiation, even a little amount (0.1 g) of this sample can accomplish a MO degradation ratio of nearly 100% within 140 min. On the other hand, almost no degradation of MO was detected in the presence of 200-0 SnS_2 without illumination (i.e., in the dark experiment) or in the absence of 200-0 SnS_2 with illumination (i.e., in the blank experiment) for 140 min. Thus, it is inferred that the degradation of MO is dominatingly a photocatalytic process, and 200-0 SnS_2 can

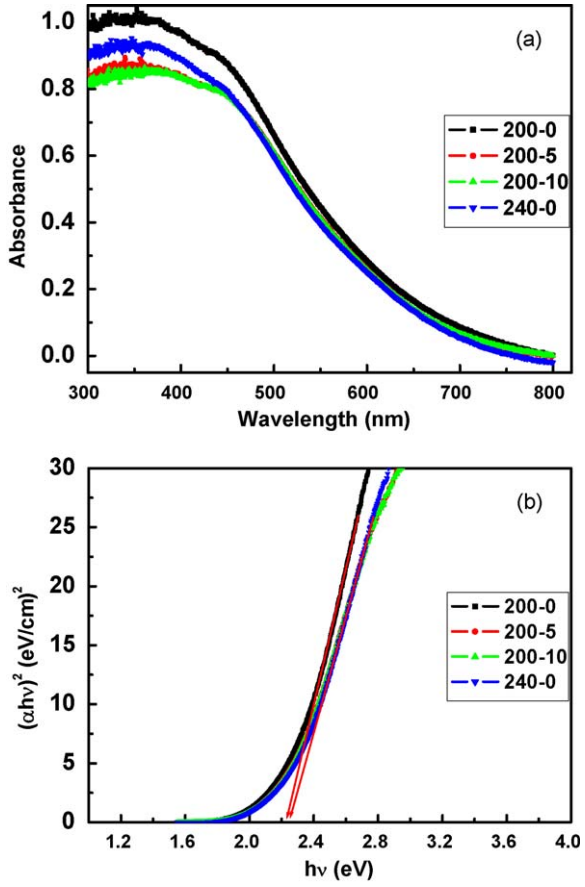

Fig. 5. (a) UV–vis diffuse reflectance spectra, and (b) plots of $(\alpha h\nu)^2$ against $(h\nu)$ for the SnS_2 products.

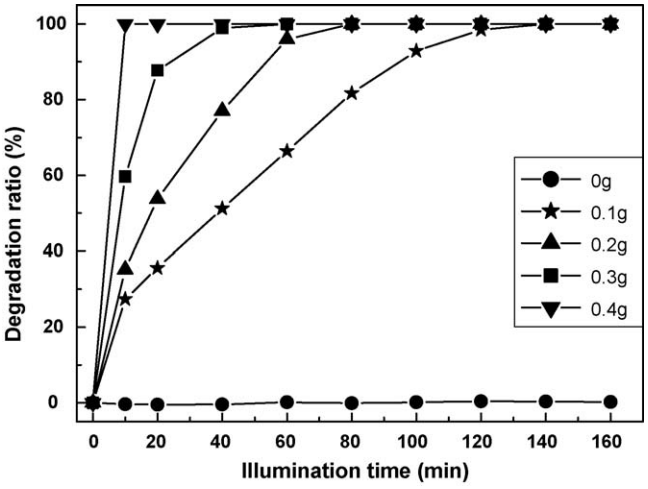

Fig. 7. Degradation evolution of MO over different amounts of 200-0 SnS_2 under the visible light ($\lambda > 420$ nm) irradiation.

efficiently promote this process. Besides, as shown by the XRD pattern in Fig. 2(e) and Raman spectrum in Fig. 4(e), hexagonal phase SnS_2 is retainable after the fifth cycle photocatalysis, further confirming that 200-0 SnS_2 acts as photocatalyst in the process of photodegrading MO.

Since the stability of sulfide photocatalysts has always been a concern, it is important to investigate the stability and repeatability of the as-synthesized SnS_2 nanoflakes in photocatalytic degradation of aqueous MO. So, in our work, 200-0 SnS_2 is recycled for five times in the same photocatalytic reactions under the visible light ($\lambda > 420$ nm) irradiation. After each cycle which lasts for 120 min, the photocatalyst is separated from the suspension by filtration, washed with hot deionized water, dried and weighed for a new cycle. Taking into account the mass loss of photocatalyst during each cycle, the fourth cycle must be conducted twice in order to accumulate enough sample for the fifth cycle, the third cycle must be conducted twice in order to accumulate enough sample for the fourth cycle, and so on. Fig. 8(a) shows the degradation evolution of MO over 0.3 g of 200-0 SnS_2 under the visible light irradiation in the first and third cycle. Obviously, the photocatalytic performance of 200-0 SnS_2 deteriorates with more recycling times. However, because of the high photocatalytic activity of 200-0 SnS_2 and certain degree of photochemical stability (that is, hexagonal phase SnS_2 can be maintained after the fifth cycle photocatalysis as revealed by the XRD pattern in Fig. 2(e) and Raman spectrum in Fig. 4(e)), it is still able to achieve a 100% degradation ratio of MO in the first three cycles, and 86% in the fifth cycle after 120 min illumination (Fig. 8(b)). The deterioration in the photocatalytic performance of semiconducting sulfides with more recycling times or prolonging reaction times was a common problem, and had been ascribed to the anodic decomposition (or the so-called photocorrosion) [29–31].

Fig. 9 shows the degradation evolution of MO in the absence or presence of photocatalysts (including 200-0 SnS_2 and P25 TiO_2) under the real sunlight irradiation. As can be seen, in the absence of any photocatalyst, the degradation of MO hardly occurs when subjected to the real sunlight irradiation for 180 min. In contrast, the degradation rates of MO under the real sunlight irradiation can be immensely accelerated by adding small amounts of 200-0 SnS_2 or P25 TiO_2. Moreover, the more amounts of 200-0 SnS_2 are added, the higher degradation ratios of MO can be achieved for a certain sunlight irradiation time until the complete degradation of MO. For example, the degradation ratios of MO over 0.2, 0.3 and 0.4 g of 200-0 SnS_2 are around 29.9%, 48.6% and 78.2%, and 45.8%, 86.9% and 97.3%, respectively, when subjected to the real sunlight irradiation for 10 and 20 min. However, for P25 TiO_2, the degradation rates of MO over different amounts of this photocatalyst follow the order of 0.3 g > 0.4 g > 0.2 g. For instance, the degradation ratios of MO over 0.2, 0.3 and 0.4 g of P25 TiO_2 are around 20.5, 30.7 and 27.2%, and 78.1, 94.1 and 86.4%, respectively, when subjected to the real sunlight irradiation for 20 and 100 min. This indicates that P25 TiO_2 has an optimum loading amount in catalytic degradation of aqueous MO under solar irradiation, which is in agreement with many previous works [25–28]. It is commonly believed that in the heterogeneous photocatalytic degradation of organic pollutants over P25 TiO_2, an increase in catalyst amount increases the number of active sites on the photocatalyst surface, which in turn increase the number of hydroxyl and superoxide radicals responsible for the oxidation decomposition of azo dyes [25–28]. Once the concentration of the catalyst increases above the optimum value, the photodegradation rate decreases due to unfavourable light scattering and reduction of light penetration into the suspension. In addition, the increase of catalyst concentration beyond the optimum may result in the agglomeration and sedimentation of catalyst particles, causing part of the catalyst surface unavailable for photon absorption and dye adsorption, and accordingly bringing little stimulation to the catalytic reaction. The aforementioned phenomena also imply that

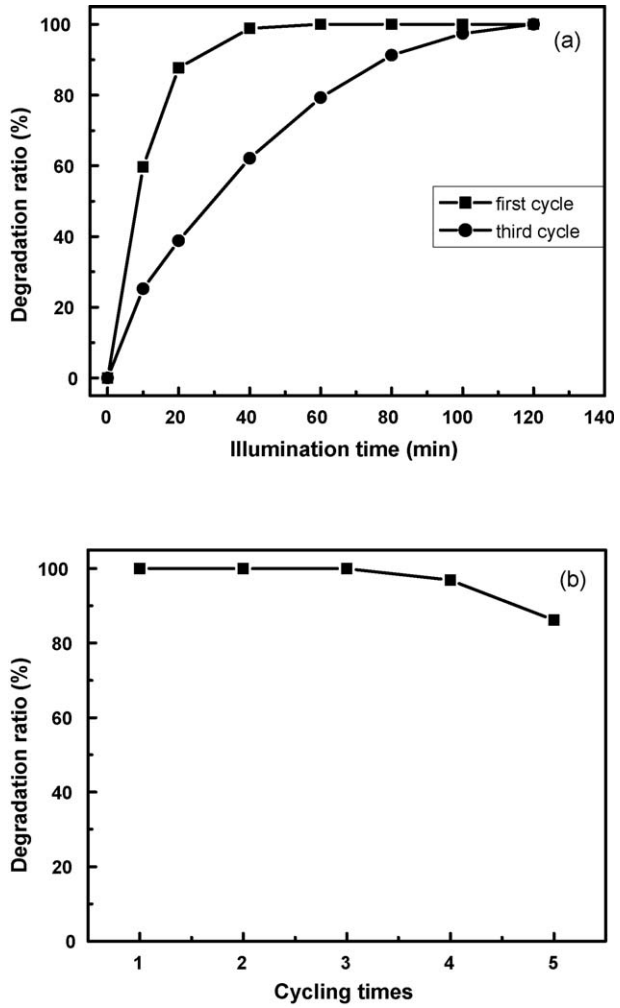

Fig. 8. (a) Degradation evolution of MO over 0.3 g of 200-0 SnS_2 under the visible light ($\lambda > 420$ nm) irradiation in the first and third cycle; and (b) the degradation ratios of MO over 0.3 g of 200-0 SnS_2 at 120 min illumination for the first five cycles.

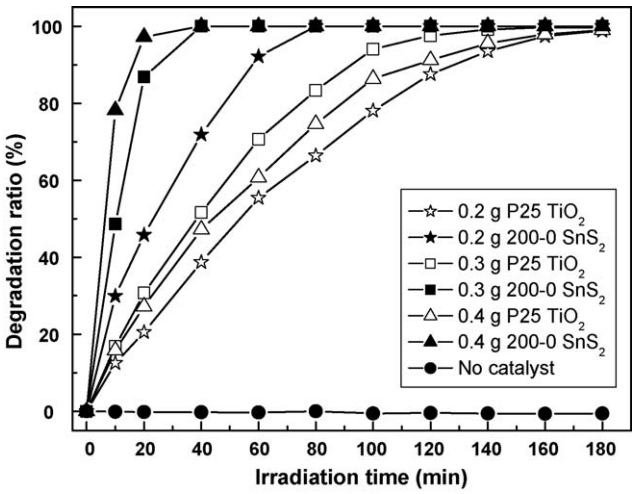

Fig. 9. Degradation evolution of MO in the absence or presence of photocatalysts (including 200-0 SnS_2 and P25 TiO_2) under the real sunlight irradiation.

200-0 SnS_2 and P25 TiO_2 need different optimum dosages for photocatalytic degradation of MO in aqueous solution under the real sunlight irradiation.

It is quite wonderful to see that 0.2–0.4 g of 200-0 SnS_2 invariably demonstrate superior photocatalytic capability to the same amounts of P25 TiO_2 in the whole process of decomposing MO under the real sunlight irradiation. To our knowledge, this is the first study of the photocatalytic activity of SnS_2-based semiconductors under the real sunlight irradiation, and the as-synthesized SnS_2 nanoflakes are among the few photocatalysts having higher photocatalytic efficiencies than P25 TiO_2 under the real sunlight irradiation by far [31,32]. Furthermore, compared with P25 TiO_2, 200-0 SnS_2 has better sedimentation ability and can be more easily separated from the suspension by filtration after the photocatalytic reactions (e.g., the recovery efficiency of 200-0 SnS_2 is above 90% for each cycle). The high sunlight photocatalytic activity, certain degree of photochemical stability and easy recovery by filtration from suspension suggest that the as-synthesized SnS_2 nanoflakes may be a promising photocatalyst in removing the organic pollutants from wastewater.

4. Conclusions

Without the assistance of template and vacuum environment/inert gas protection, bulk-pure hexagonal phase SnS_2 nanoflakes were synthesized simply via heating the mixture of $SnCl_2{\cdot}2H_2O$ and excess S powders in air at 200–240 °C for 0–10 h, coupled with a subsequent washing treatment. The proposed method is simple, mild and cheap, which may be suitable for large-scale production of multifunctional SnS_2 nanopowder. Furthermore, the as-synthesized SnS_2 nanoflakes not only showed a much superior photocatalytic activity to Degussa P25 TiO_2 toward the degradation of aqueous MO under the real sunlight irradiation, but also can be easily recovered from the suspension by filtration after the photocatalysis, which makes them a prospective photocatalyst in remediation of water polluted by some chemically stable organic dyes.

Acknowledgements

This work is supported by the University Natural Science Foundation of Jiangsu Province (No. 08KJB150019), and the National Natural Science Foundation of China (No. 50873085).

Appendix A. Supplementary data

Supplementary data associated with this article can be found, in the online version, at doi:10.1016/j.apcatb.2009.12.022.

References

[1] S. Rehman, R. Ullah, A.M. Butt, N.D. Gohar, J. Hazard. Mater. 170 (2009) 560–569.
[2] H. Yamashita, M. Harada, J. Misaka, M. Takeuchi, B. Neppolian, M. Anpo, Catal. Today 84 (2003) 191–196.
[3] T. Kamegawa, J. Sonoda, K. Sugimura, K. Mori, H. Yamashita, J. Alloy Compd. 486 (2009) 685–688.
[4] Z. Bian, Y. Huo, Y. Zhang, J. Zhu, Y. Lu, H. Li, Appl. Catal. B: Environ. 91 (2009) 247–253.
[5] C. Yang, W. Wang, Z. Shan, F. Huang, J. Solid State Chem. 182 (2009) 807–812.
[6] C. Wang, K. Tang, Q. Yang, Y. Qian, Chem. Phys. Lett. 357 (2002) 371–375.
[7] N.G. Deshpande, A.A. Sagade, Y.G. Gudage, C.D. Lokhande, J. Alloy Compd. 436 (2007) 421–426.
[8] S.K. Panda, A. Antonakos, E. Liarokapis, S. Bhattacharya, S. Chaudhuri, Mater. Res. Bull. 42 (2007) 576–583.
[9] D. Ma, H. Zhou, J. Zhang, Y. Qian, Mater. Chem. Phys. 111 (2008) 391–395.
[10] N. Takeda, B.A. Parkinson, J. Am. Chem. Soc. 125 (2003) 5559–5571.
[11] J. Seo, J. Jang, S. Park, C. Kim, B. Park, J. Cheon, Adv. Mater. 20 (2008) 4269–4273.
[12] T.-J. Kim, C. Kim, D. Son, M. Choi, B. Park, J. Power Sources 167 (2007) 529–535.
[13] H. Mukaibo, A. Yoshizawa, T. Momma, T. Osaka, J. Power Sources 119–121 (2003) 60–63.
[14] P.W. Shen, J.T. Wang, Dictionary of Compounds, Shanghai Lexicographical Publishing House, Shanghai, 2002.
[15] W. Shi, L. Huo, H. Wang, H. Zhang, J. Yang, P. Wei, Nanotechnology 17 (2006) 2918–2924.
[16] Y. Lei, S. Song, W. Fan, Y. Xing, H. Zhang, J. Phys. Chem. C 113 (2009) 1280–1285.
[17] H. Xiao, Y.C. Zhang, Mater. Chem. Phys. 112 (2008) 742–744.
[18] H. Xiao, Y.C. Zhang, H. Bai, Mater. Lett. 63 (2009) 809–811.
[19] Q. Yang, K. Tang, C. Wang, D. Zhang, Y. Qian, J. Solid State Chem. 164 (2002) 106–109.
[20] X.L. Gou, J. Chen, P.W. Shen, Mater. Chem. Phys. 93 (2005) 557–566.
[21] B. Hai, K. Tang, C. Wang, C. An, Q. Yang, G. Shen, Y. Qian, J. Cryst. Growth 225 (2001) 92–95.
[22] A.R. Wang, H. Xiao, Mater. Lett. 63 (2009) 1221–1223.
[23] K.-Q. Li, F.-Q. Huang, X.-P. g Lin, Scripta Mater. 58 (2008) 834–837.
[24] Y. Liu, Y.C. Zhang, X.F. Xu, J. Hazard. Mater. 163 (2009) 1310–1314.
[25] I.K. Konstantinou, T.A. Albanis, Appl. Catal. B 49 (2004) 1–14.
[26] U.G. Akpan, B.H. Hameed, J. Hazard. Mater. 170 (2009) 520–529.
[27] U.I. Gaya, A.H. Abdullah, J. Photochem. Photobiol. C 9 (2008) 1–12.
[28] M.A. Rauf, S.S. Ashraf, Chem. Eng. J. 151 (2009) 10–18.
[29] H. Yang, C. Huang, X. Li, R. Shi, K. Zhang, Mater. Chem. Phys. 90 (2005) 155–158.
[30] L.B. Reutergårdh, M. Langphasuk, Chemosphere 35 (1997) 585–596.
[31] B. Neppolian, H.C. Choi, S. Sakthivel, B. Arabindoo, V. Murugesan, J. Hazard. Mater. 89 (2002) 303–317.
[32] M. Muruganandham, M. Swaminathan, Sol. Energy Mater. Sol. Cells 81 (2004) 439–457.